CHAPTER IV

RESULT AND VALIDATION OF THE PROGRAM

Solar flux density distribution on the cylindrical surface is simulated by using MATHLAB program. Our simulation results are sun position, mirror position and heliostat field, mirror orientation, principal image on image plane, flux dimensionless calculation, and the determination of flux density distribution on the receiver plane. Validations of these results are presented in this chapter.

4.1 Sun Position

The sun position can be calculated following the standard technique (see equations 3.2 and 3.3). The calculated sun position is compared with the result from the EZ Cosmos computer program. Figure 4.1(a) and 4.1(b) show a comparison between our calculation of sun position on 29 July and the result from EZC program. The absolute relative errors are lower than 0.04 % in solar azimuth and altitude angle.

For most time of the year, the sun rises in the south-east and sets in the south-west of Bangkok. In Thailand, the 105° E longitude is taken as the reference longitude. The standard time for Thailand at 105° E is ahead of the Greenwich Mean Time (GMT) by 7 hours. Bangkok is at the longitude 100.5° E. When the sun is overhead at noon at the longitude 105° E, it appears to be due east as seen from Bangkok. It takes the sun 4 minutes to traverse one degree of longitude, so that it

completes 360 degree in 24 hours. It takes another 18 minutes for the sun to appear overhead above Bangkok. For the location at 105° E, the solar time and the local time are virtually identical. The solar time is the time coincident with the position of the sun.

Bangkok is situated at latitude 13.7° north and longitude 100.5° east. For Bangkok, the sun is due north at noon on June 21st and the sun is due south on December 21st. Table 4.1 shows the altitude and azimuth angles of the sun for daytime on the four different days.

The projection of the sun's path on the horizontal plane is called a sun-path diagram. Such diagram is very useful in predicting flux density distribution on the cylindrical surface. The solar altitude can then be read from the concentric circles in the diagram; the azimuth from the scale around the circumference of the diagram. Figure 4.2 shows the sun path diagram for Bangkok for the 1st of every month.

Table 4.1: Solar altitude (ϕ) and azimuth (Ψ) angles for Bangkok on the four days

Solar Time (hour)	Mar 21 and Sept 21		June 21		December 21	
	ϕ (degree)	Ψ (degree)	ϕ (degree)	Ψ (degree)	ϕ (degree)	Ψ (degree)
06.00	0.00	89.60	5.42	112.85	0.00	67.15
08.00	28.94	81.75	32.69	109.26	20.55	58.02
10.00	57.09	66.97	60.02	113.34	42.63	38.57
12.00	75.86	0.00	80.29	180.00	52.81	0.00
14.00	57.09	293.02	60.02	246.66	42.63	321.43
16.00	28.94	278.24	32.69	250.74	20.55	301.95
18.00	0.00	270.39	5.42	247.15	0.00	292.84

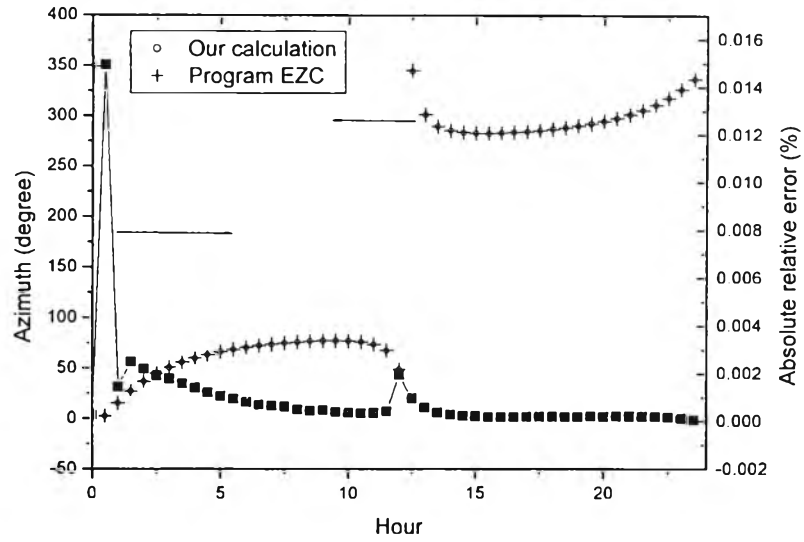

(a): Sun azimuth angle on 29 July

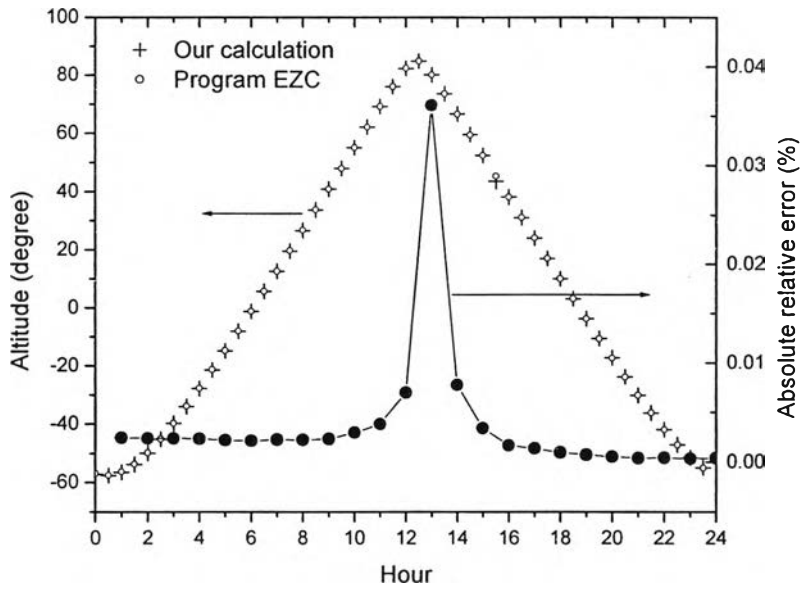

(b) Sun altitude angle on 29 July

Figure 4.1: Example of sun position calculation from our program compared with EZC program .

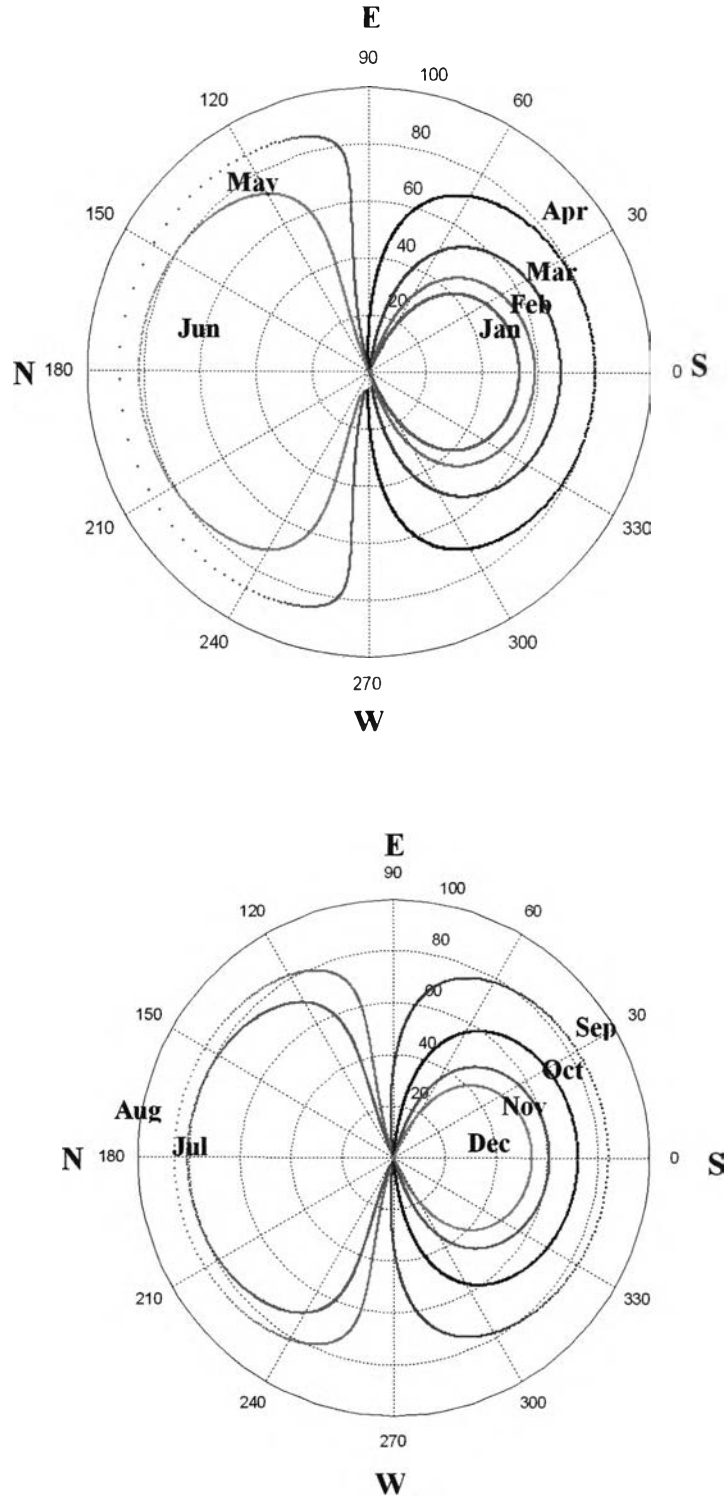

Figure 4.2: The sun path diagram for the observation at 13.6° N latitude and 100.5°E longitude represents the position of the sun based on the altitude and the azimuth.

4.2 Mirror Position and Heliostat Field

The layout of heliostat field is optimized for the most packing and non-blocking principle. The size of mirror when placed perpendicular to the earth surface is chosen to be 0.3 m in width and 0.2 m in height. The result of calculation for optimum heliostat arrangements is shown in table 4.2 [15]. The minimum distances from heliostat to the tower of all case are 5.0 m. The result shows that, total number of heliostats in field depend on terrain slope. Blocking effect could be reduced by such slope. Maximum number of heliostats in one quadrant is 1,507 when terrain slop is 5 degree.

Figure 4.3 shows the layout of heliostat field used in this calculation with the terrain slope of 0 degree. It consists of 5,844 mirrors placed into 36 circles around the central tower the center of which is 10 m above the ground. Figure 4.4 shows all mirrors image when being observed from the top of the tower. Non-overlapping mirror confirms the no-blocking principle.

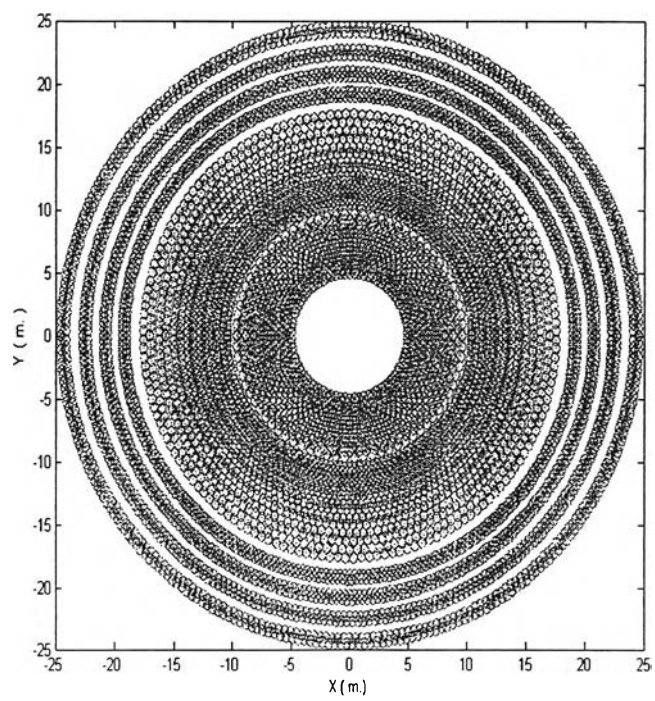

Figure 4.3: Heliostat field layouts for no-blocking radial staggered distribution [15]

Table 4.2: Result of calculation for optimum heliostats arrangements [15]

Terrain Slope (degree)	No. of heliostats	Rmax (m.)	Rmin (m.)	No. of Heliostats/area	No. of groups	No. of ring			Total group
						Group 1	Group 2	Group 3	
0.0	1461	24.558	5.0	3.216	3	14	14	8	36
0.5	1461	24.503	5.0	3.231	3	14	14	8	36
1.0	1457	24.449	5.0	3.237	3	14	14	8	36
1.5	1388	23.431	5.0	3.371	3	15	12	8	35
2.0	1388	23.383	5.0	3.385	3	15	12	8	35
2.5	1388	23.337	5.0	3.399	3	15	12	8	35
3.0	1441	24.723	5.0	3.128	3	15	14	7	36
3.5	1441	24.673	5.0	3.141	3	15	14	7	36
4.0	1431	24.624	5.0	3.132	3	15	14	7	36
4.5	1431	24.576	5.0	3.145	3	15	14	7	36
5.0	1507	24.962	5.0	3.206	3	15	14	8	37
5.5	1442	24.000	5.0	3.330	3	14	14	8	36
6.0	1442	23.954	5.0	3.343	3	14	14	8	36
6.5	1438	23.910	5.0	3.347	3	14	14	8	36
7.0	1438	23.865	5.0	3.360	3	14	14	8	36
7.5	1438	23.822	5.0	3.373	3	14	14	8	36
8.0	1431	23.780	5.0	3.369	3	14	14	8	36
8.5	1427	23.738	5.0	3.372	3	14	14	8	36
9.0	1427	23.698	5.0	3.384	3	14	14	8	36
9.5	1427	23.660	5.0	3.395	3	14	14	8	36
10.0	1427	23.624	5.0	3.406	3	14	14	8	36

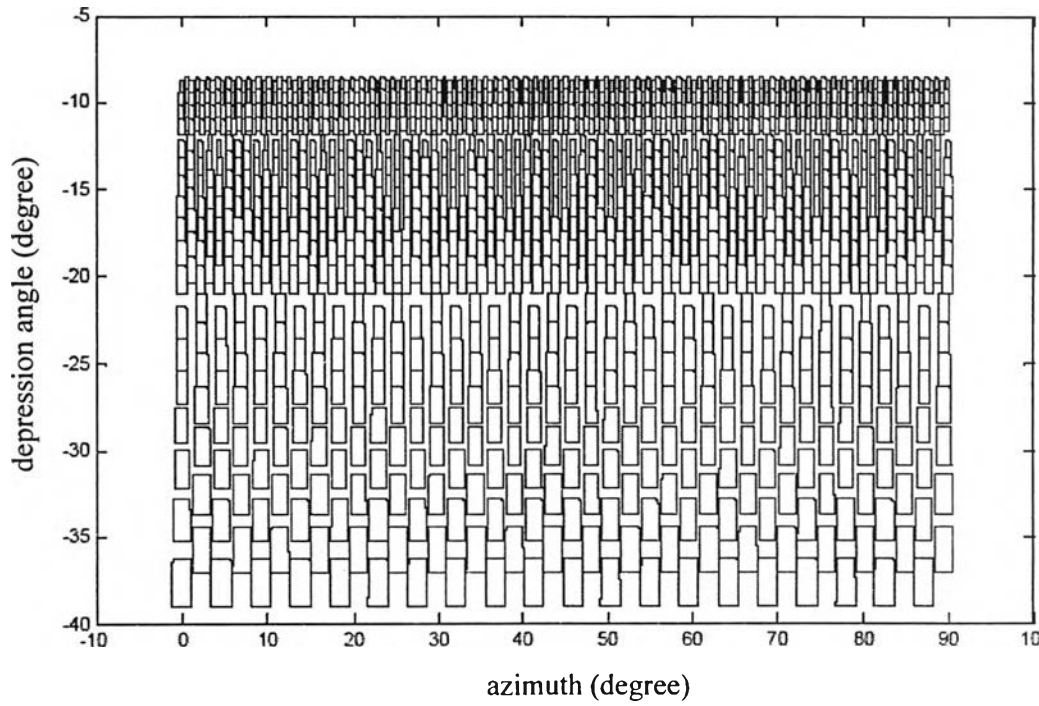

Figure 4.4: Mirrors as seen from the receiver [15]

4.3 Mirror Orientation

A rotational matrix is formulated to be used for controlling the normal vector of the mirror. It is validated by comparing with M.R.Riaz's result [16]. Figure 4.6 shows time profiles of angular orientations for seven mirrors placed into a ring at the tower altitude (θ_r) 60 degree. The chosen day is the equinox ($\delta = 0$ degree) and the latitude is 35° N. Figure 4.6 (b) shows the mirror azimuth angle. Negative mirror azimuth means that the mirror rotates from south to east directions and vice versa.

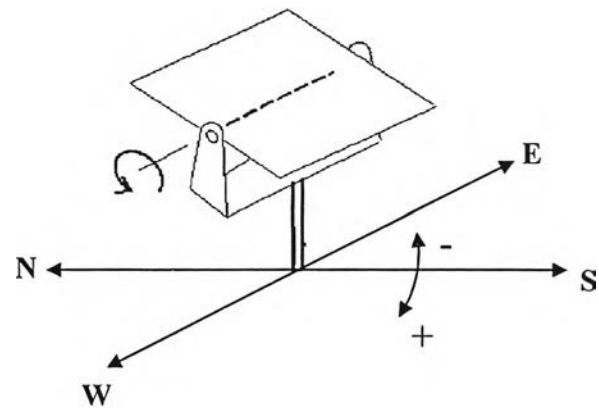

Figure 4.5: Mirror azimuth angle measured with respect to the south, positive value in westward direction and negative in eastward direction (after M.R.Riaz [16])

These figures are calculated by our program compare with M.R.Riaz. The result of calculation, mirror altitude and mirror azimuth are same shape and same value when compared with M.R.Riaz.. It is confirming our work that correct.

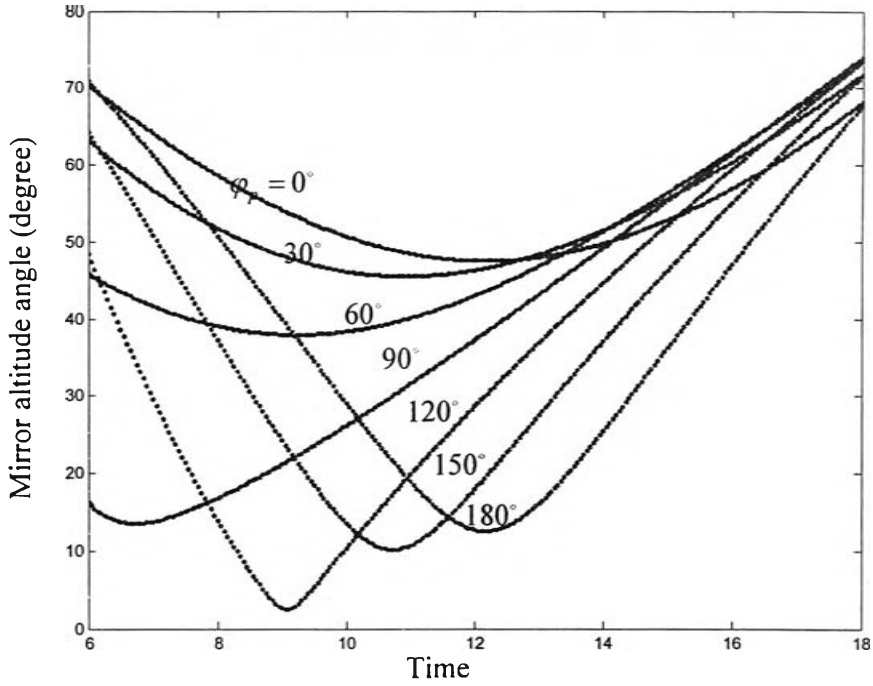

(a)

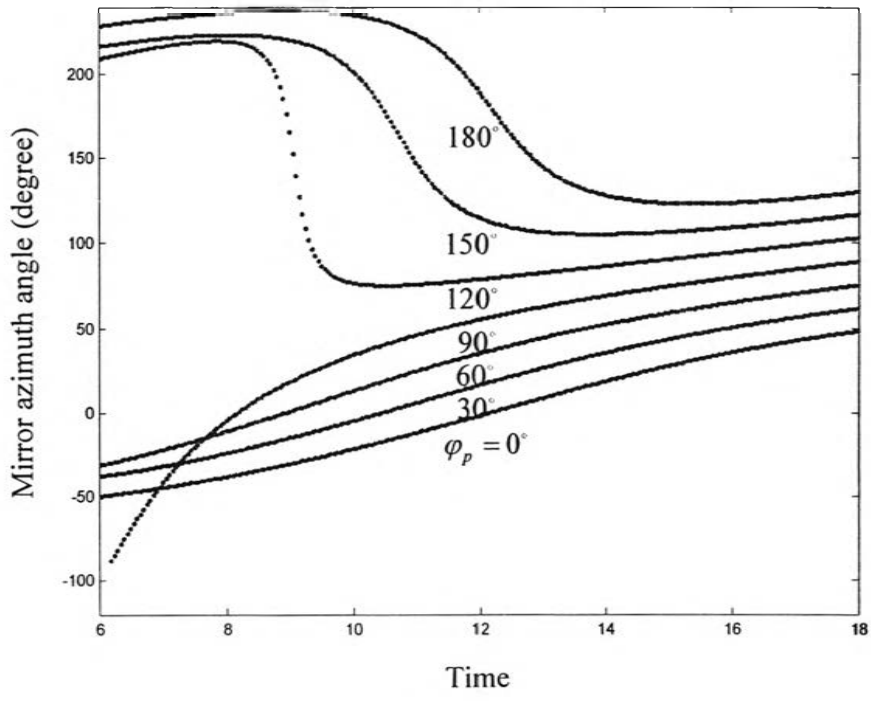

(b)

Figure 4.6: Time profile of mirror altitude and mirror azimuth angle

4.4 The Principal Image on the Image Plane

The amount of direct radiation intercepted by a surface depends on the incidence angle. Figure 4.7 shows the incidence angle for a mirror surface tilted at altitude angle α_m from the horizontal and mirror azimuth angle φ_m measured from south in eastward direction.

$$\cos\theta_i = \cos\alpha_m \cos\theta_z + \sin\alpha_m \sin\theta_z \cos(\Psi - \varphi_m) \tag{4.1}$$

The principal image area is defined as an effective area and calculated as a function of position and time by ray tracing technique. This technique is more useful than equation 4.1 because we know effective area and coordinate of four corners of area. The principal image is validated by comparing the result with that of M.M. Elsayed and K.A. Fathalah [13]. Figures 4.8 and 4.9 show the length of principal image sides, L'_H and L'_T . L'_H is the ratio of L_H to D_H which is normalized to the radius of solar disk. Similarly, L'_T is the ratio of L_T to D_T which is normalized to the radius of solar disk. They depend greatly on sun altitude (α), $\Psi - \varphi_p$, and r_h / H . L'_H is maximum when the mirror position is in the same or opposite direction of the sun position ($\Psi - \varphi_p$ = 0 or 180 degree). L'_T is maximum when the mirror position is in opposite direction to the sun position ($\Psi - \varphi_p$ = 180 degree) and its minimum when mirror position is same direction the sun position ($\Psi - \varphi_p$ = 0 degree). Figure 4.10 shows the angle θ^* between two sides of the principal image. It is between 53 and 127 degree for $\alpha \geq 50$ degree and $r_h / H \leq 10$. θ^* is negative when measured in clockwise manner and positive when measured anticlockwise manner. θ^* is maximum when mirror position is in the opposite direction to the sun position ($\Psi - \varphi_p$ = 180 degree) and is minimum when mirror position is same direction to the sun position.

Figures 4.8 to 4.10 show that the heliostats opposite to the sun give higher effective area than those in the same direction with the sun. This result is confirmed by our calculation in Figure 4.11.

The ratio of effective area to total area for each month, chosen on the 1st day of month is shown in Figure 4.12.

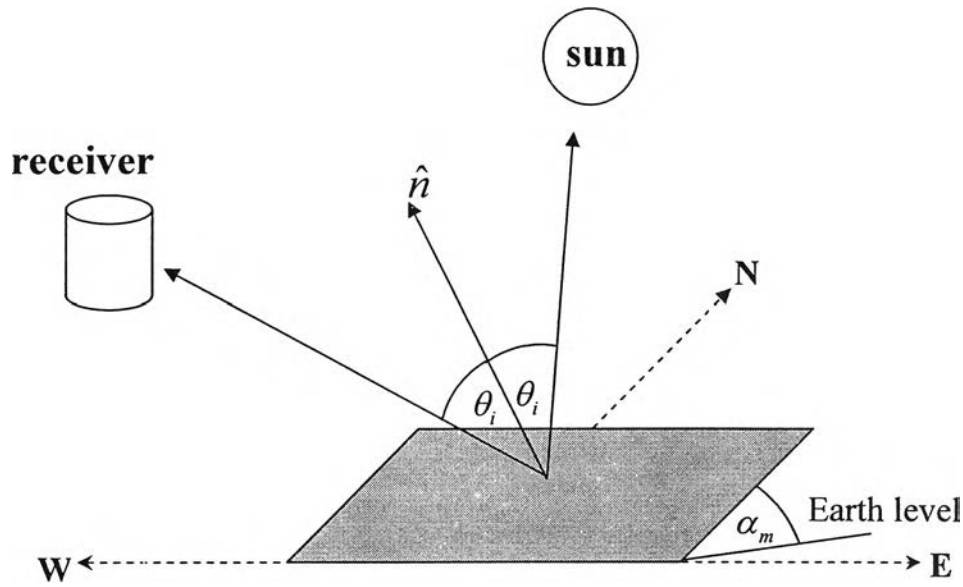

Figure 4.7: Definition of incidence angle

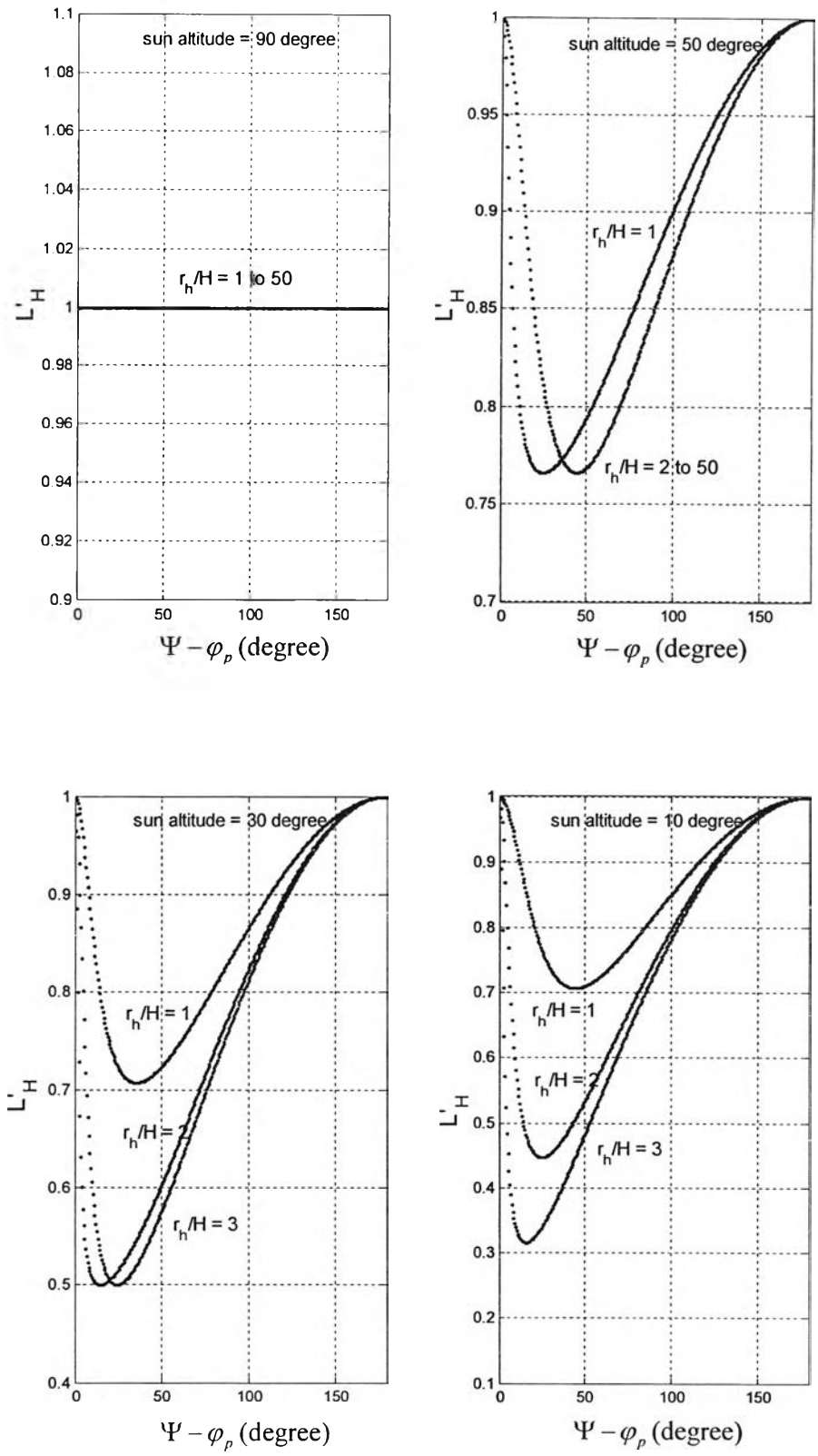

Figure 4.8: Variation of L'_H with $r_h / H, \alpha$ and $\Psi - \varphi_p$

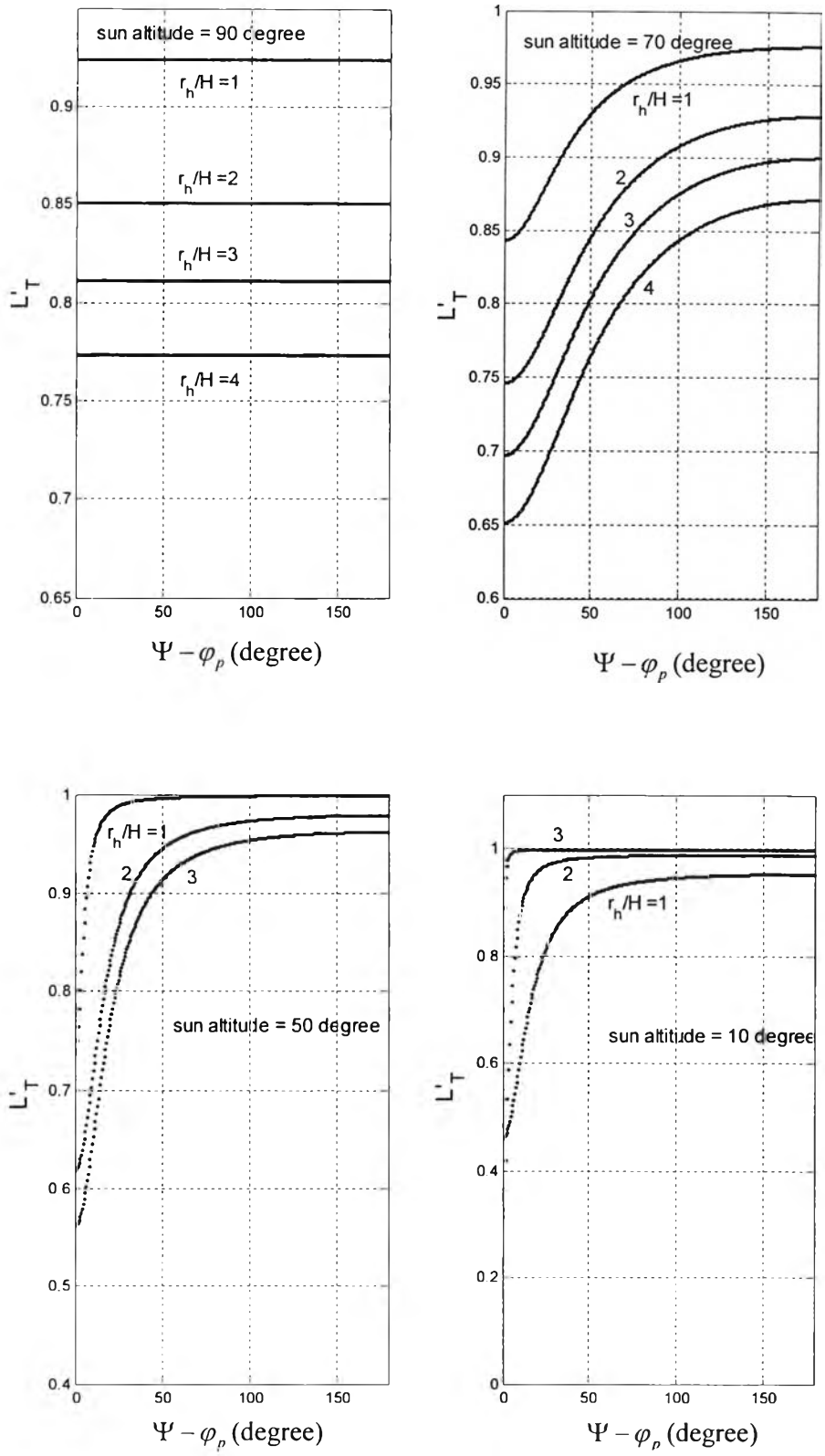

Figure 4.9: Variation of L'_T with $r_h / H, \alpha$ and $\Psi - \varphi_p$

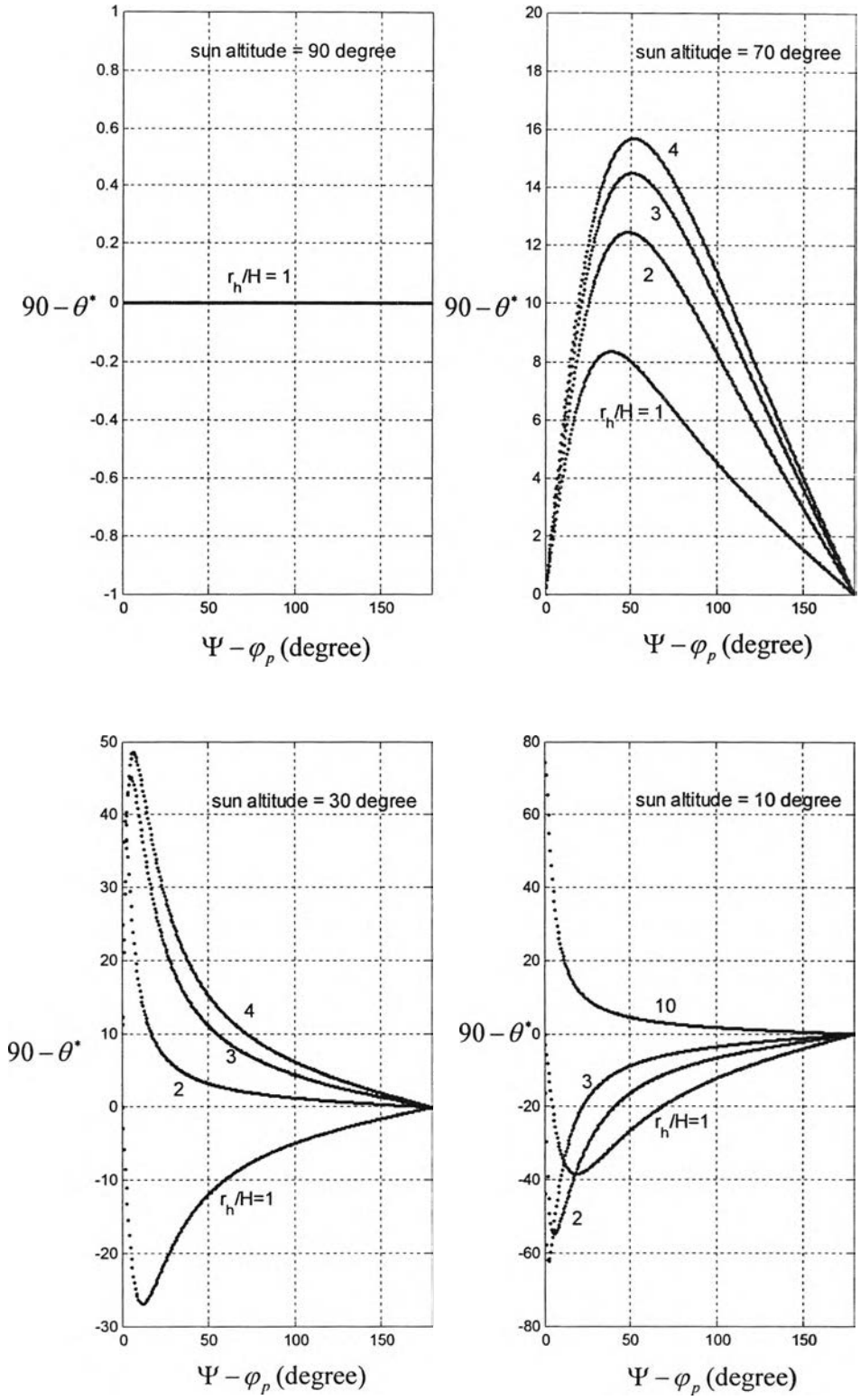

Figure 4.10: Variation of θ^* with $r_h / H, \alpha$ and $\Psi - \varphi_p$

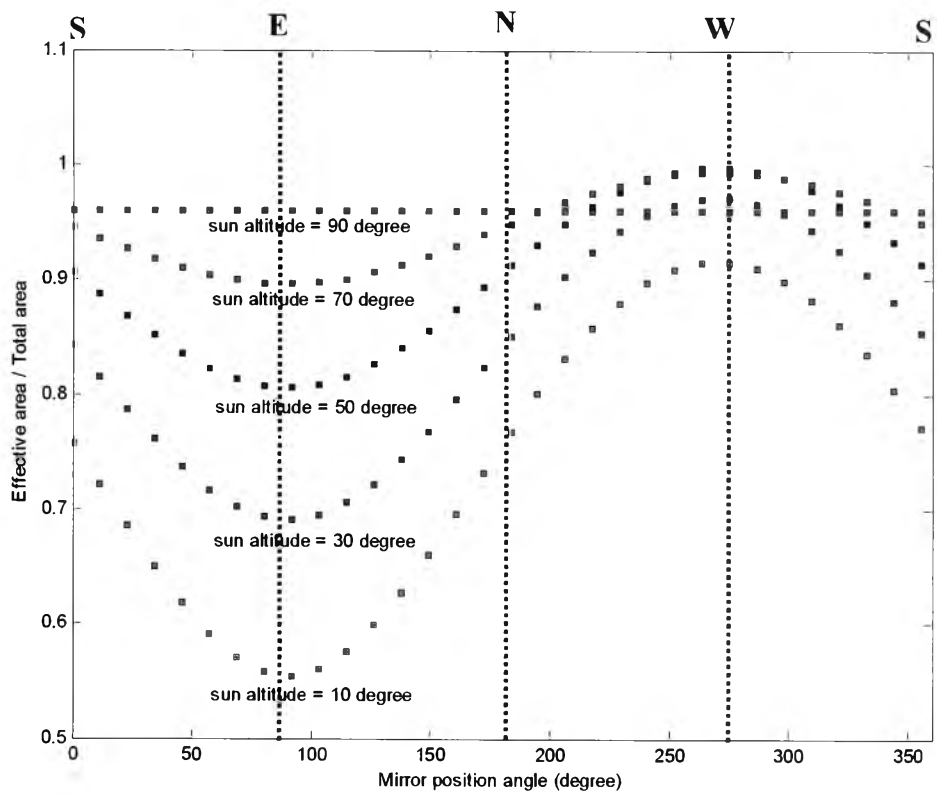

Figure 4.11: The effective area of the mirror placed at 5 m from the central tower. The sun azimuth is assumed 90 degree (East)

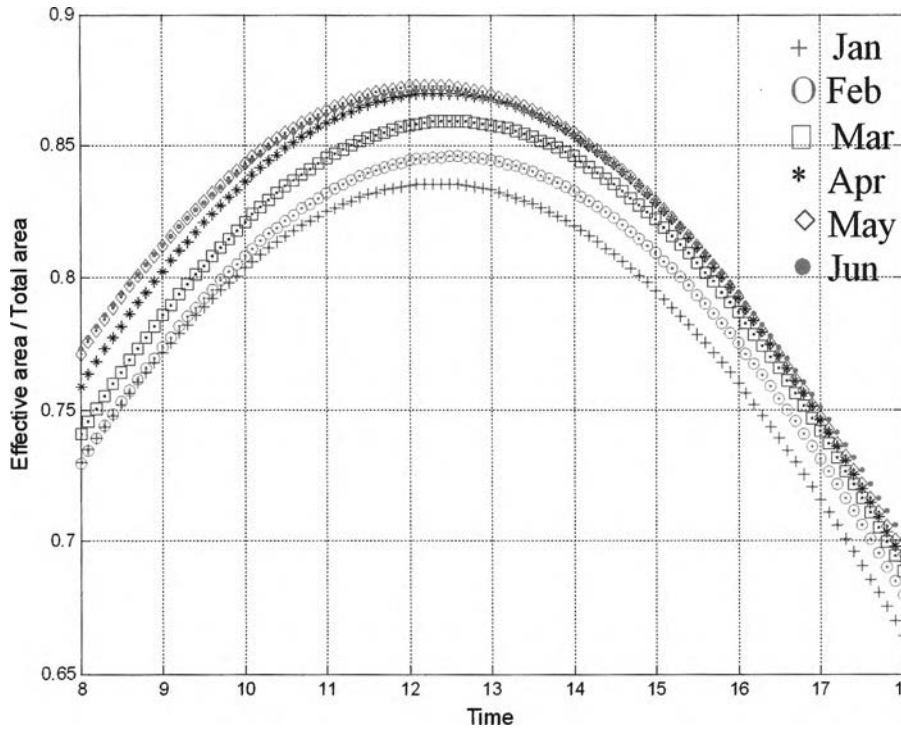

(a)

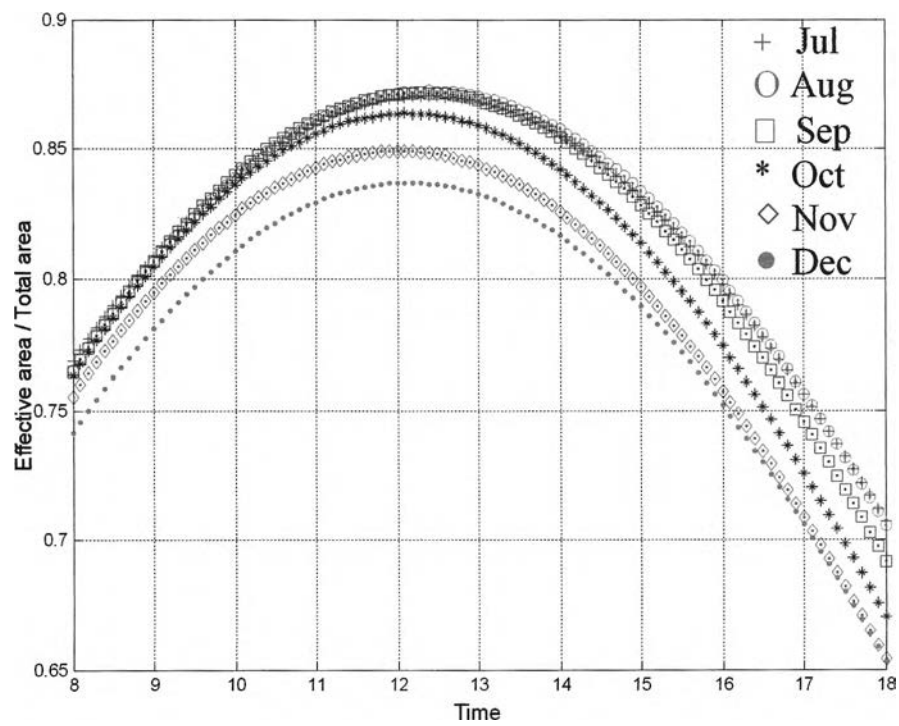

(b)

Figure 4.12: The ratio of effective area to total area of heliostat field, chosen on the 1st of each month

Table 4.3: Incidence angle and comparison of effective area between rays tracing technique and calculate by equation 4.1

Day/month	Time	Mirror position (X,Y,Z)	Incidence angle (degree)	Ratio of effective area to mirror area	
				Ray tracing	By equation 4.1
1/1	8.00	(0,5,1)	24.5912	0.6483	0.6483
1/1	8.00	(0,-5,1)	35.0052	0.9083	0.9083
1/2	10.00	(0.39957,4.98401,1)	41.3142	0.7983	0.7983
1/2	10.00	(-0.39957,4.98401,1)	40.8522	0.8150	0.8150
1/2	10.00	(-0.39957,-4.98401,1)	10.9480	0.9700	0.9700
1/2	10.00	(0.39957,-4.98401,1)	13.7842	0.9600	0.9600
1/7	14.00	(1.57283,4.74618,1)	37.8519	0.9983	0.9983
1/7	14.00	(-1.57283,4.74618,1)	42.0289	0.9850	0.9850
1/7	14.00	(-1.57283,-4.74618,1)	75.6290	0.8900	0.8900
1/7	14.00	(1.57283,-4.74618,1)	74.7697	0.9066	0.9066

4.5 Flux Dimensionless Calculation

The separation of variable and superposition technique is used to determine the flux density distribution on the receiver plane of a central receiver system. The first step of the calculation is to determine the flux density distribution on the image plane. The distribution on image plane is calculated from the algebraic sum of several flux distribution functions (see equation 3.24). Each of these functions is determined in terms of basic dimensionless flux density function Φ, transferred the origin to the corner of the principal image. The basic dimensionless flux density distribution is calculated for several value of θ^*.

Flux dimensionless for a range of ξ^* and η^* over zone 1 and $\theta^* = 90°$ is shown in Figure 4.13. It shows that flux dimensionless depend on ξ^* and η^* coordinate. If $(\xi^*, \eta^*) = (-1, -1)$, flux dimensionless is 0 because of the solar disk does not intersect with principal image. Flux dimensionless increase when ξ^* or η^* increases and it is 1 when $(\xi^*, \eta^*) = (1, 1)$. To speed up the calculation, the result of θ^* ranging from 50° to 130° with 5° steps are computed and stored as a lookup table in the computer for $-1 \le \xi^* \le 1$ and $-1 \le \eta^* \le 1$, with 0.01 m steps in both ξ^* and η^*. The tables can be used for the interpolation to determine the flux density distribution at any value of θ^*, ξ^* and η^*. The nearest value of θ^* is used. It was suggested by M.M Elsayed and K.A. Fathalah that the accuracy of this table in θ^* contributes to less than 1% of Φ.

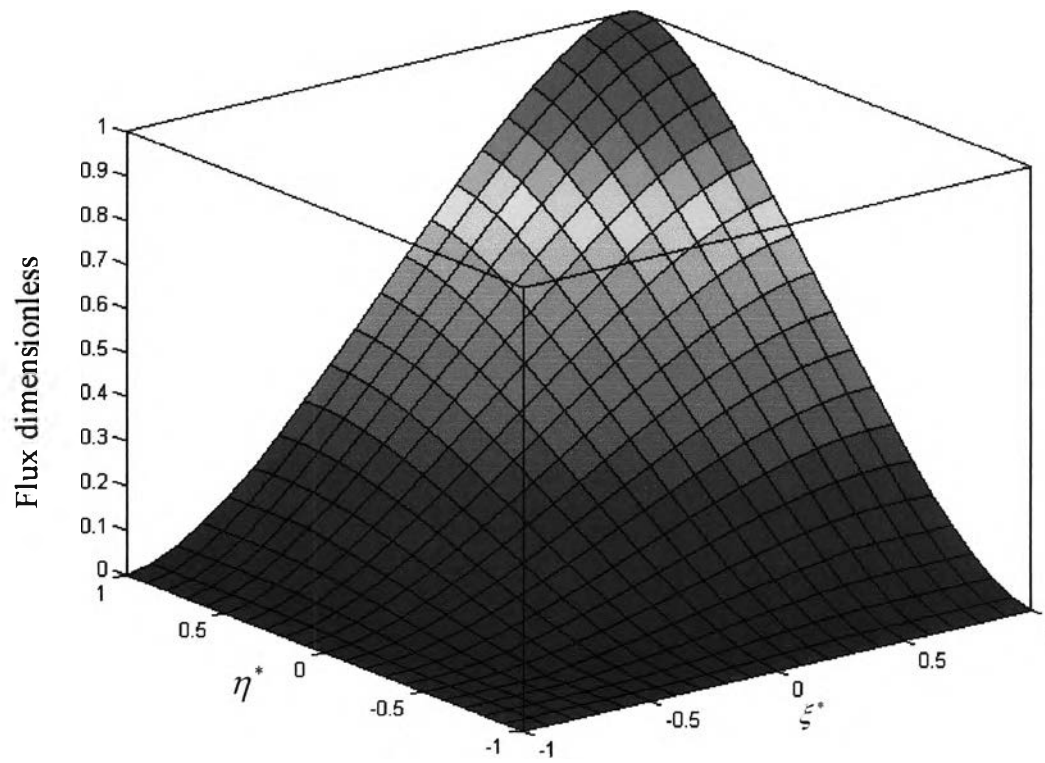

Figures 4.13: Flux dimensionless for θ^* = 90°

4.6 The Determination of the Flux Density Distribution

4.6.1 The Flux Density Distribution of a Heliostat

In the modeling of the central receiver system, it is necessary to consider the flux distribution due to a single heliostat. The method of flux distribution calculation follows section 4.5.

My work is compared with those of M.M Elsayed and K.A. Fathalah. Consider the tower height of 300 m and heliostat with $D_H = D_T = 6\,\text{m}$, located at $\varphi_p = 30$ degree and $r_h / H = 1$, for a given time with sun altitude of 40 degree and sun azimuth of 0 degree. When we compare Figure 4.14 (a) and (b), shape and maximum value of flux are the same. A better feature of our work is that the flux distribution is smoother because we can calculate with 0.01 m steps in ξ^* and η^* while M.M Elsayed and K.A. Fathalah calculate with 2 m steps in ξ^* and η^*.

For demonstration, the flux distribution of a single heliostat is shown in Figure 4.15. It is typical that the peak locates at the central area of the distribution and falls to zero at the boundaries.

As the mirror area is reduced, and the mirror is moved further away from the receiver, the value of maximum flux density decrease compared with flux density of mirror near to the tower. This is because radius of solar disk increases with the tower-to-mirror distance. Solar disk larger than principal image so flux dimensionless less than 1 (see Figures 4.16 to 4.18). When the solar disk is larger than the principal image, the flat surface changes to a smooth curve.

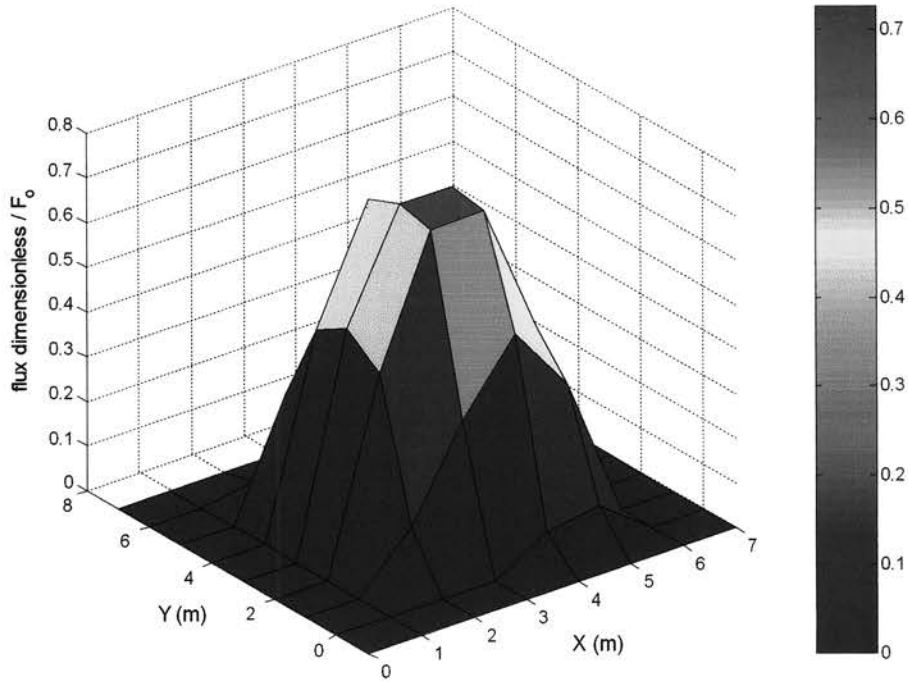

(a)

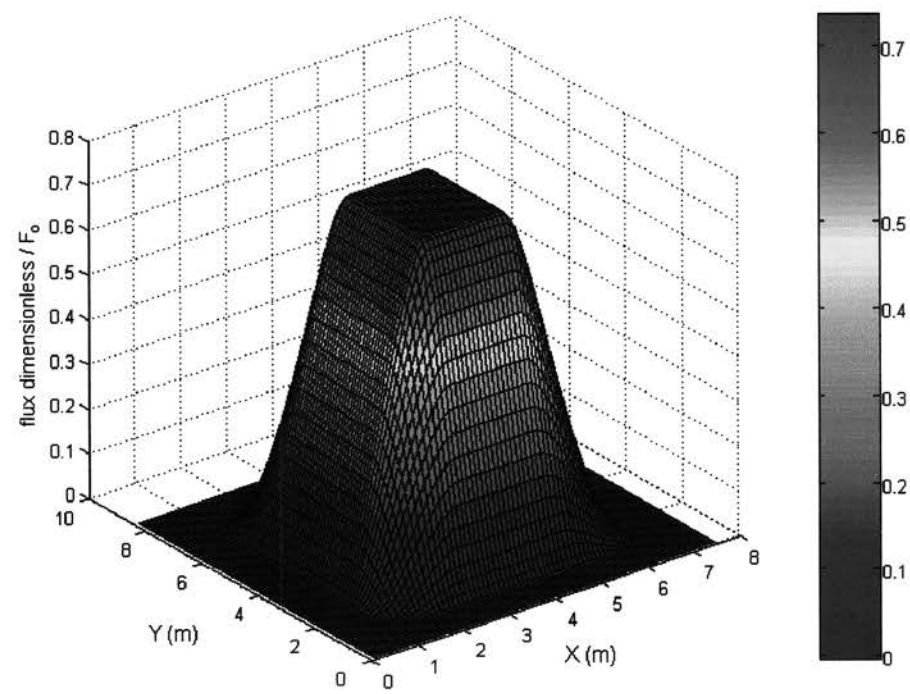

(b)

Figure 4.14: Comparisons of Flux distribution from (a) M.M Elsayed and K.A. Fathalah and (b) our work

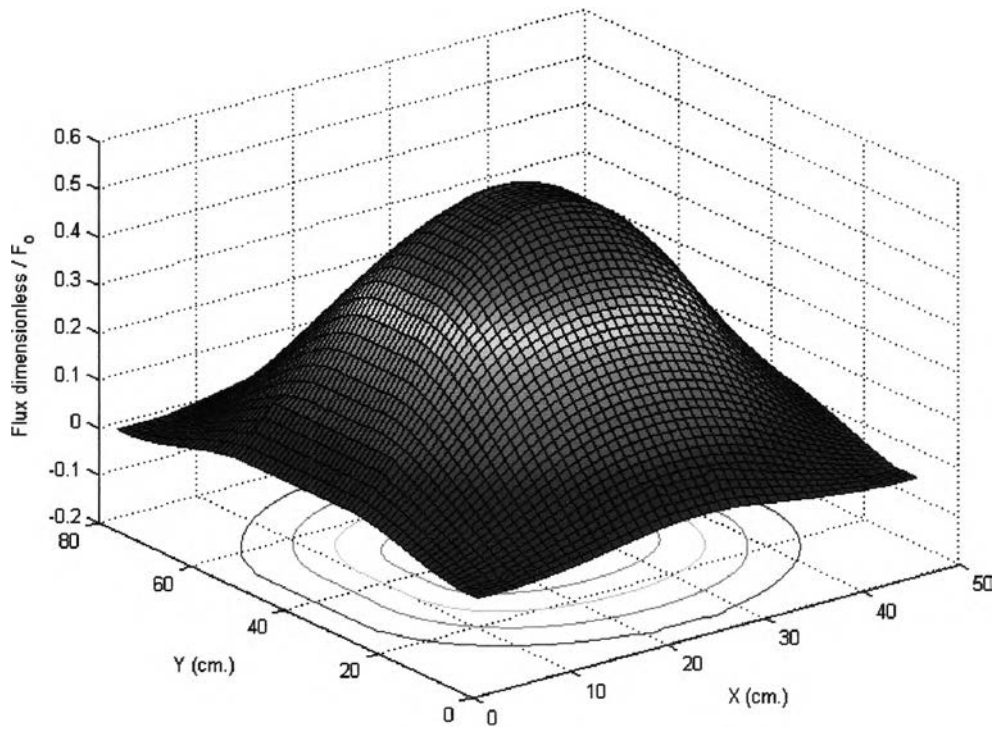

Figure 4.15: Flux dimensionless distribution on the image plane from a single rectangular heliostat. The sun elevation angle is 90 degree and the distance from the mirror to image plane is 26.59 m. The mirror size is 0.3 × 0.2 m^2. Solar flux distribution is maximum at the center of the image and falls to zero near the boundaries.

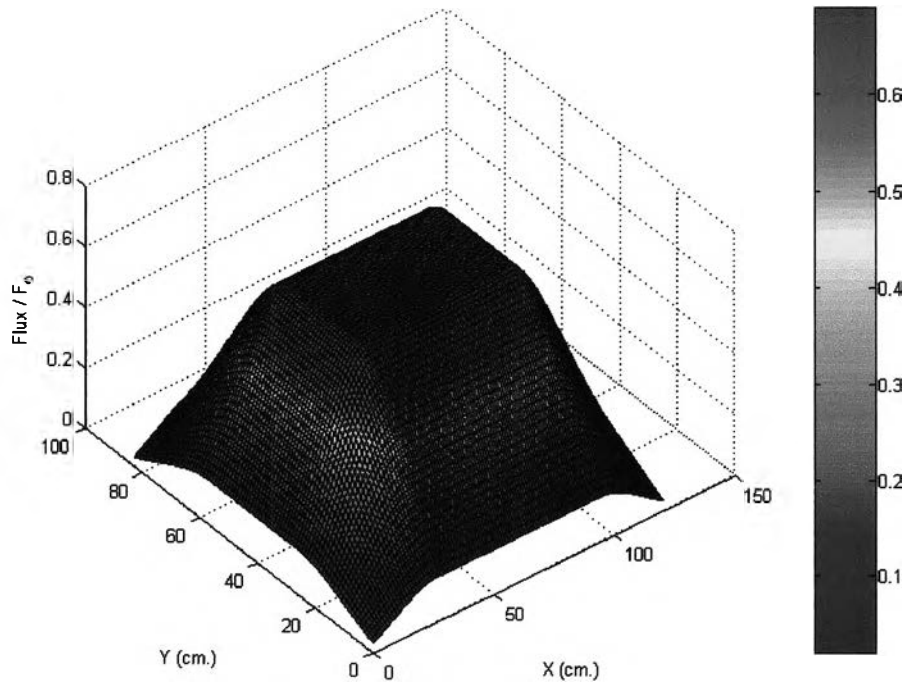

Figure 4.16: Flux dimensionless distribution on image plane when distance from the mirror to image plane is 5 m. The mirror size is 0.3×0.2 m^2.

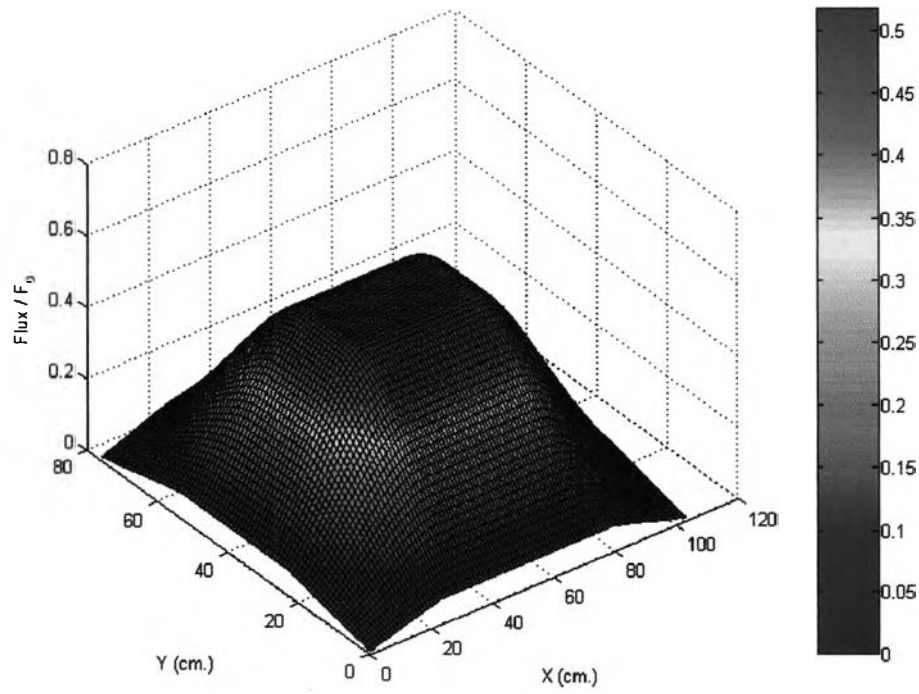

Figure 4.17: Flux dimensionless distribution on image plane when distance from the mirror to image plane is 10 m. The mirror size is 0.3×0.2 m^2.

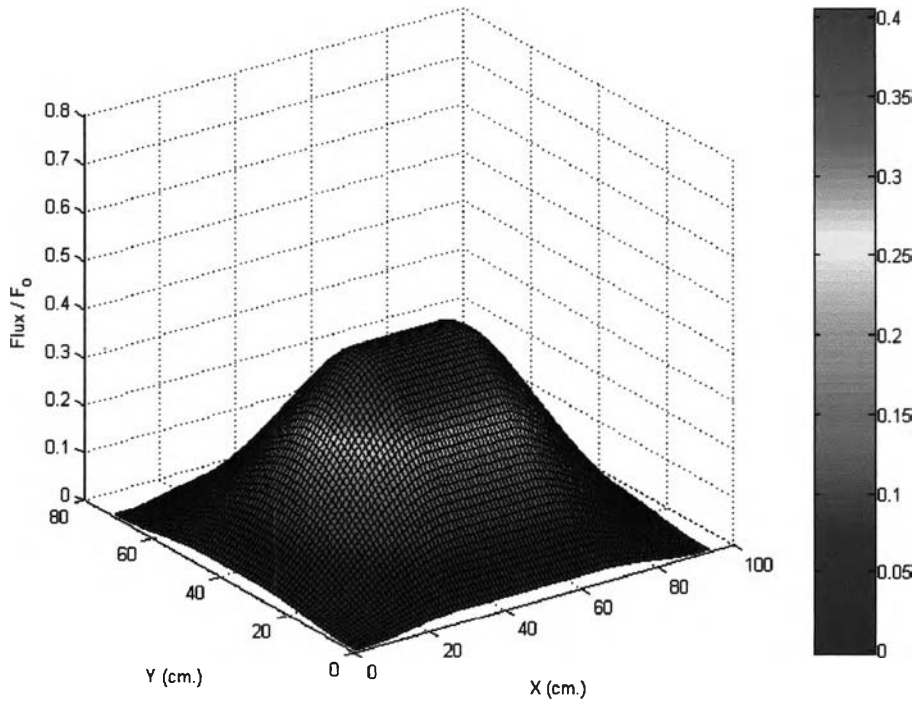

Figure 4.18: Flux dimensionless distribution on image plane when distance from the mirror to image plane is 15 m. The mirror size is 0.3×0.2 m^2.

4.6.2 The Total Flux Density Distribution on the Receiver Surface

In this section, the solar flux density distribution on an infinitely long cylindrical receiver is calculated with the mirror arrangement as shown in Figure 4.3. The results show that when the sun altitude is 90 degree, the flux distributes uniformly and radially (see Figure 4.19(a)). Figure 4.19 (b) shows that when the sun position is in the east and the sun altitude is 70 degree, the flux density distribution on the surface is minimum in the sun direction and maximum in the opposite direction. From several simulations, it can be concluded that the flux distribution be minimum in the direction of the sun.

Figure 4.20 shows the superposition of principal image of heliostats on the receiver surface. The image of the most inner ring of mirror appears at the bottom and that of the furthest ring is at the top of the picture. The most superposition is around the aim point which is at 10 m above the ground. It should be noted that the principal image of all mirrors appear to be the same regardless of their position because these images are produced from the parallel sunrays.

Figure 4.21 shows the cross section of flux distribution on cylindrical surface when the sun altitude is 90 degree. The aim point is at the center of the cylinder, 10 m above the ground. This figure shows three groups of flux distribution because of heliostat field have three groups. Image from heliostats nearest to the tower base intercept cylindrical surface lower in height than those further from the tower. The peak of solar flux density is less than 9 suns from 36 rings of heliostats. The fluctuation of width flux distribution is due to artifact of our calculation. Cylindrical surface is divided to small window, 1 degree in horizontal and 1 cm step the height in vertical. Each point of principal image on image plane is projected onto cylindrical surface. If it is a decimal, it is rounded to the nearest integers. So the flux density distribution is not smooth.

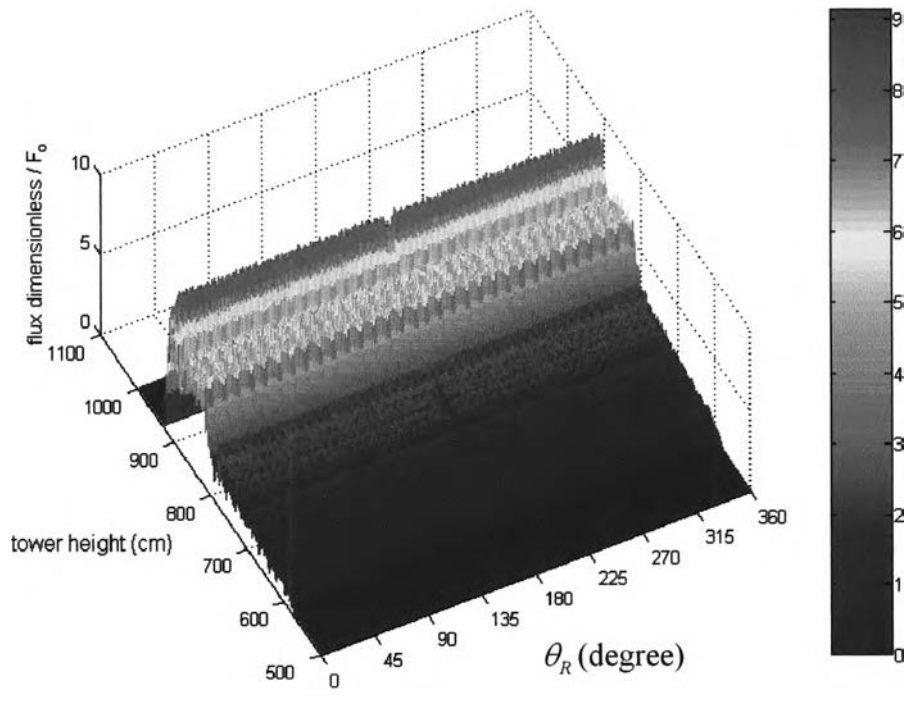

(a)

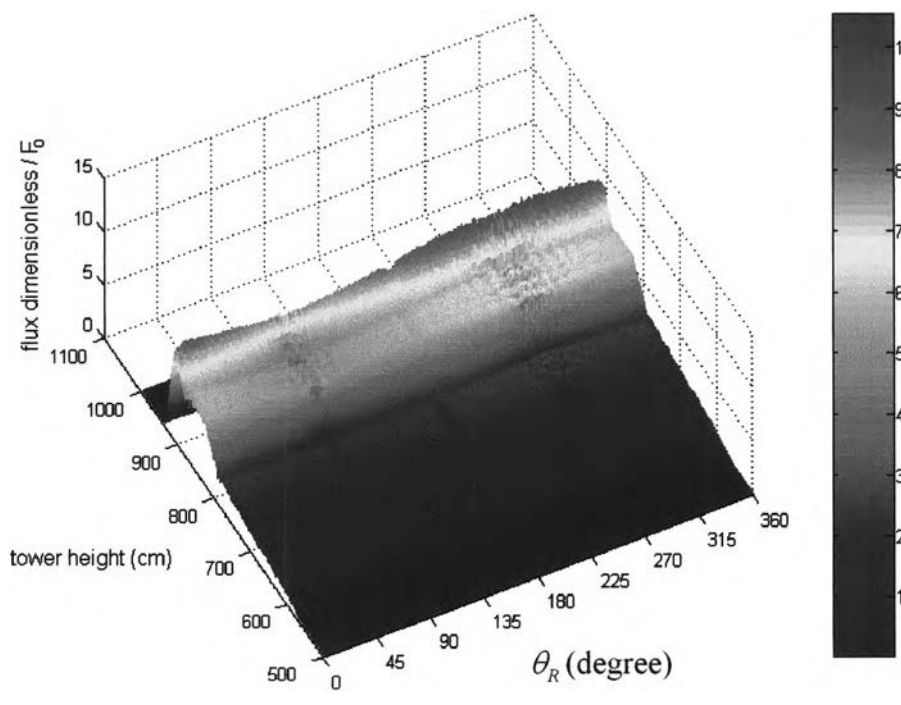

(b)

Figure 4.19: Solar flux distribution on the cylindrical surface where (a) sun altitude is 90 degree and (b) sun altitude is 70 degree. The aim height is at 1,000 cm.

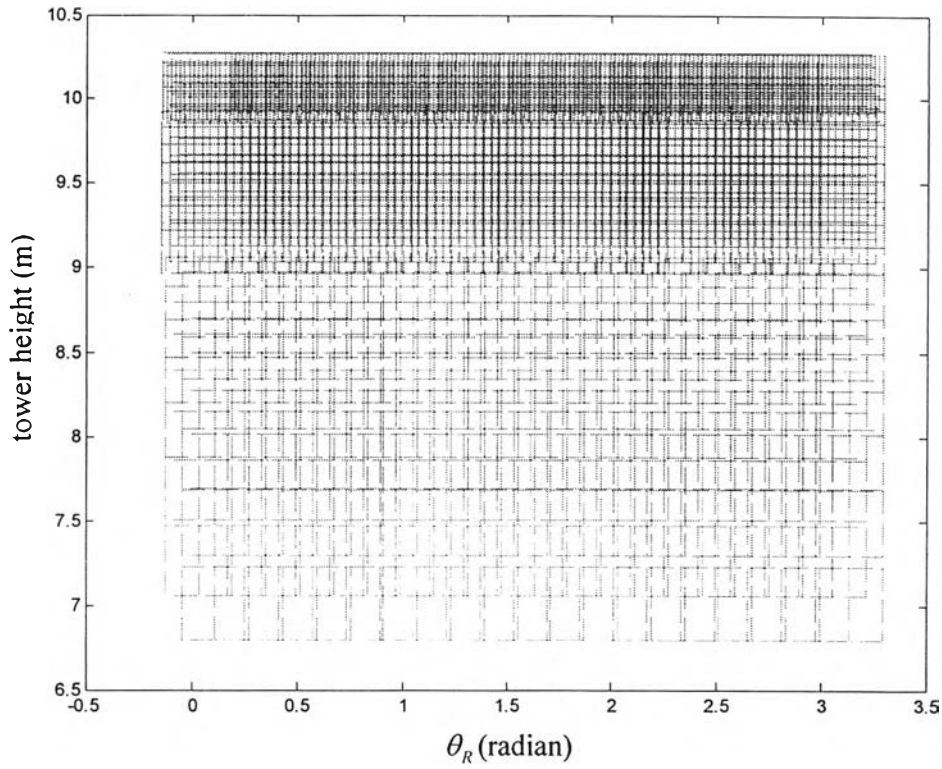

Figure 4.20: Image of mirrors in the 1st quadrant on cylindrical surface when sun altitude is 90 degree. Radius of cylinder is 2 m and aim point is 10 m above the ground.

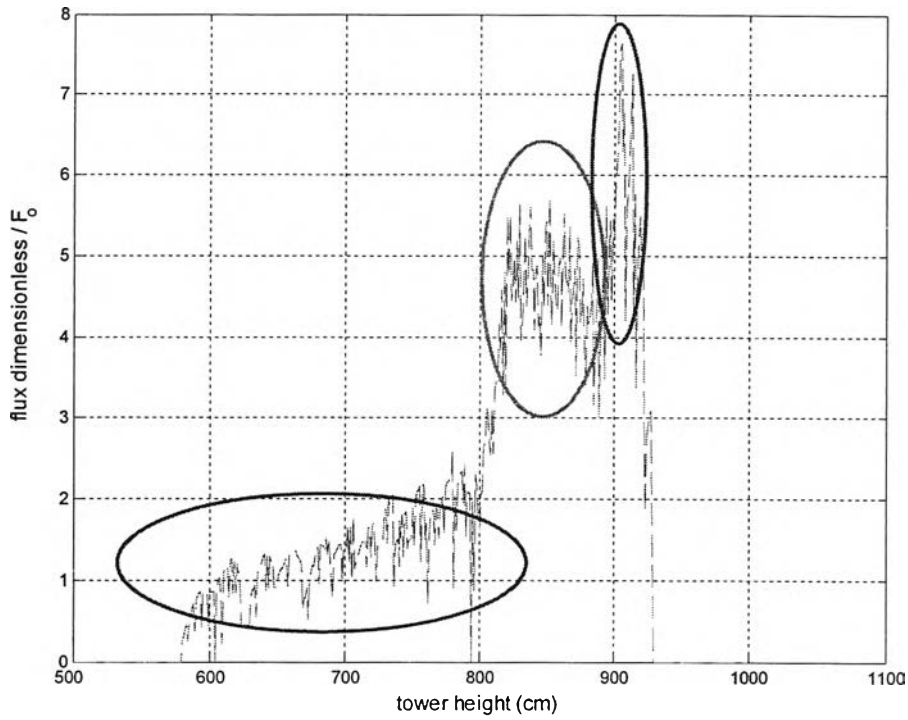

Figure 4.21: Three groups of flux distribution cross section on cylindrical surface for the sun altitude of 90 degree

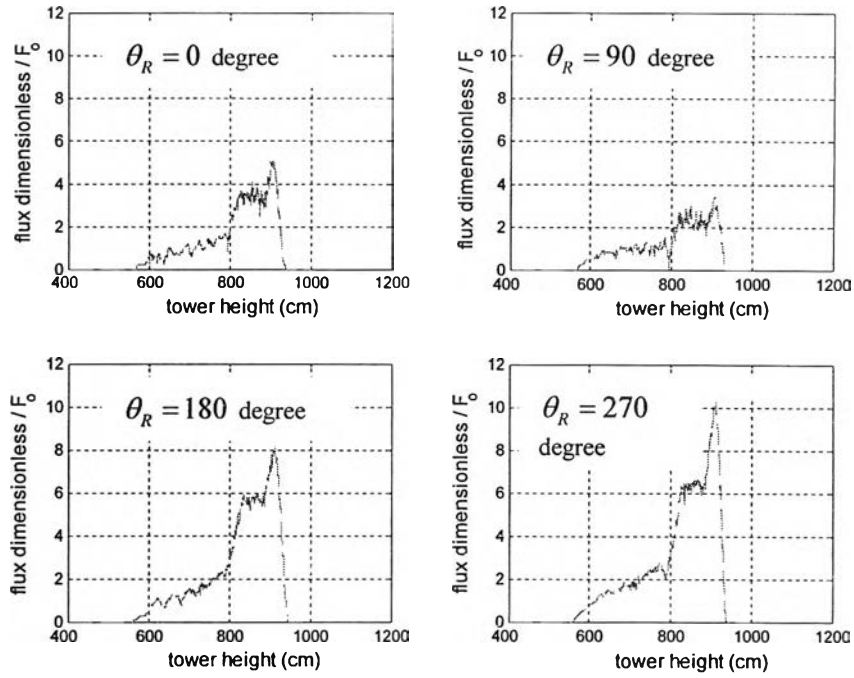

Figure 4.22: Across section of flux distribution on cylindrical surface on 1 January time at 8:00 a.m.

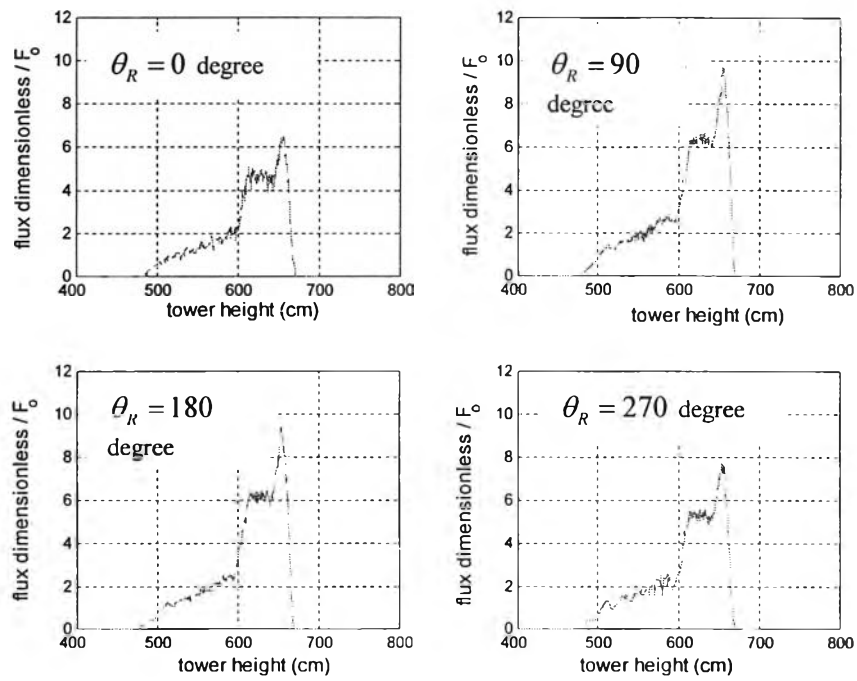

Figure 4.23: Across section of flux distribution on cylindrical surface on 1 March time at 14:00 p.m.

4.7 Multiple Aimed Points

With a single aim-point strategy, the distributions illustrated in Figures 4.21 to 4.23 spread over the cylindrical surface with maximum flux dimensionless less than the number of the heliostat rings. It is necessary to resort to multiple aiming strategies by changing aim point from the center of cylinder to surface ring of the cylinder. This strategy, each aim point of each heliostat is same height from the ground. The solar flux density can be further increased up to 60 suns.

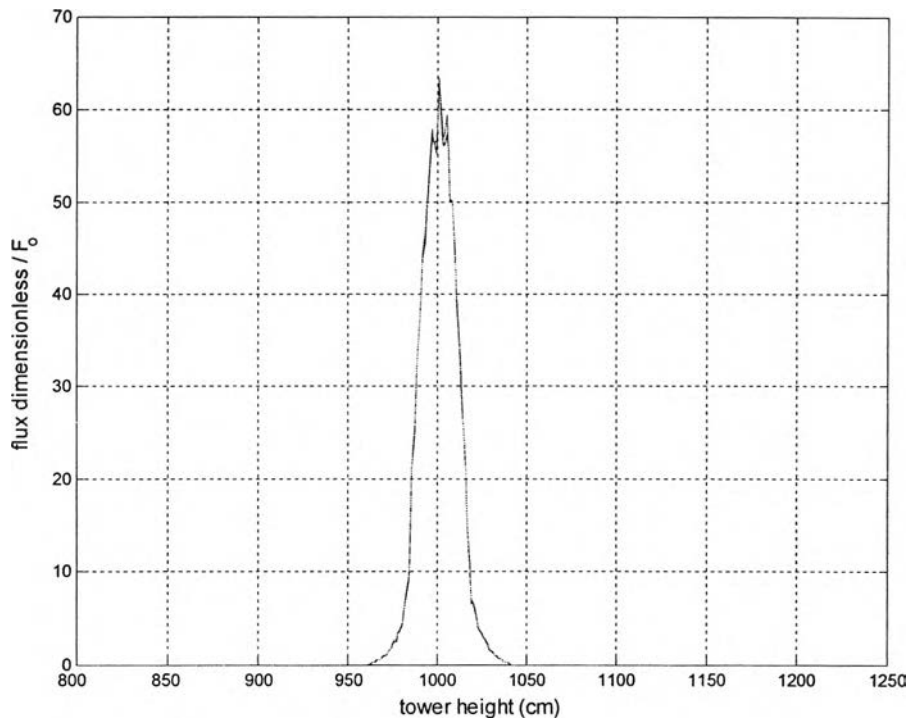

Figure 4.24: Cross section of flux distribution by multiple aim point strategies when sun altitude is 90 degree.

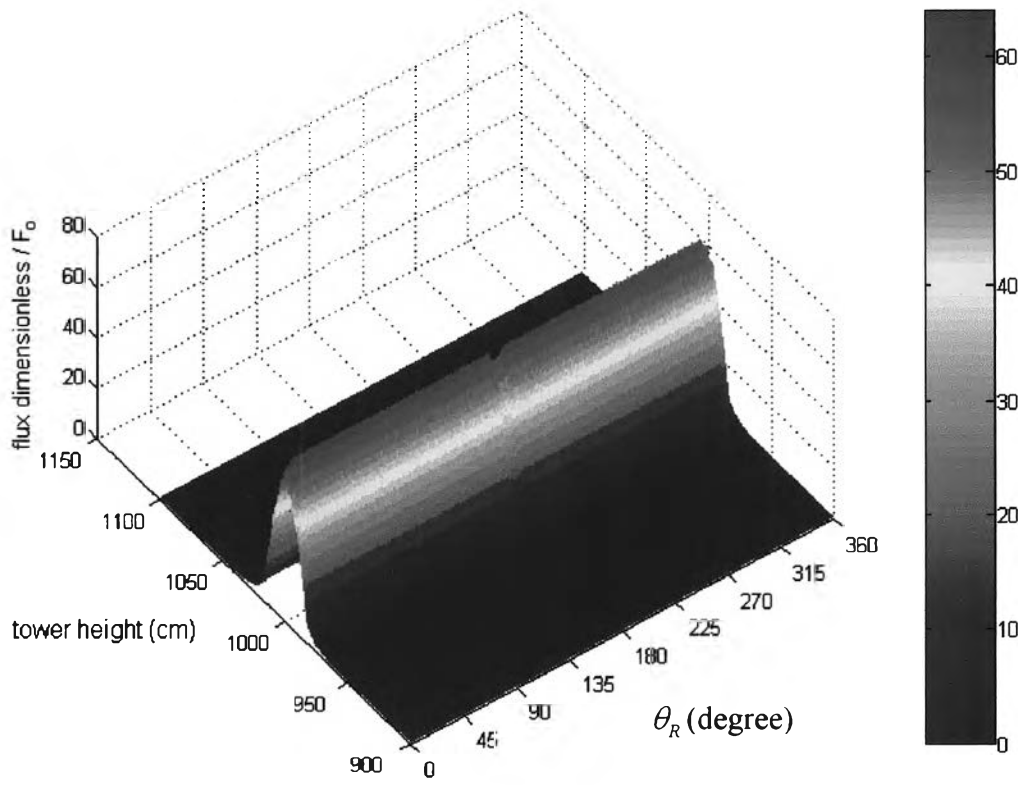

Figure 4.25: Solar flux distribution on the cylindrical surface, calculated by multiple aiming ring strategies with the sun altitude of 90 degree and the aim height of at 1,000 cm.

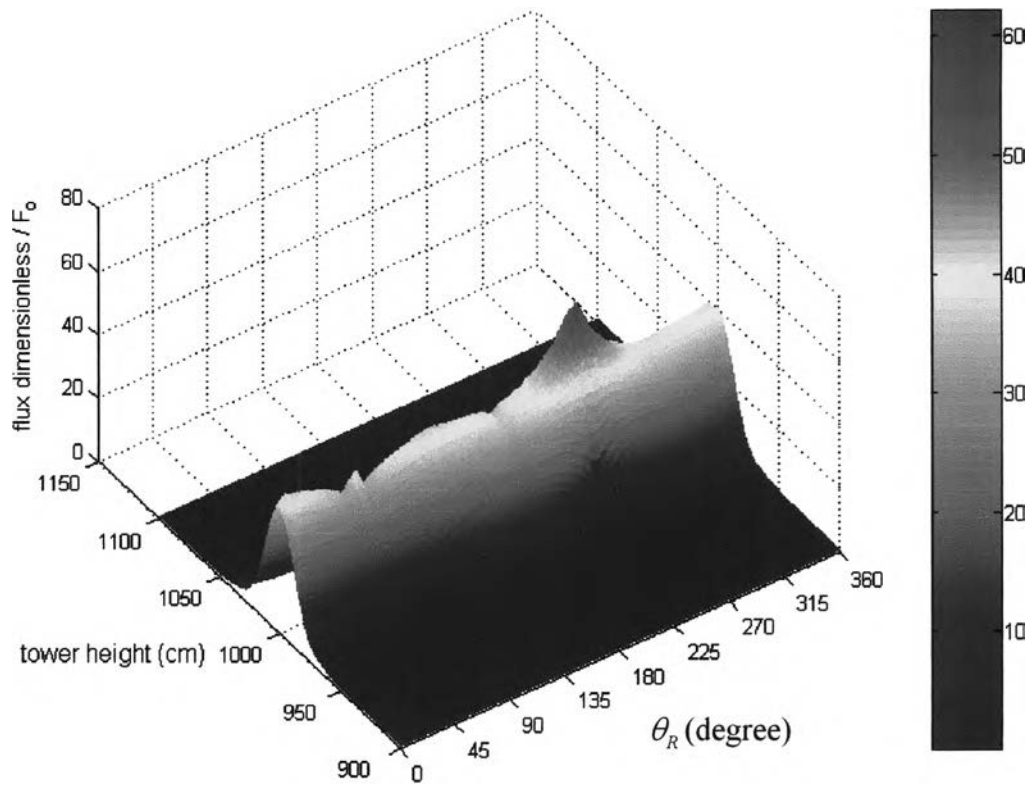

Figure 4.26: Solar flux distribution on the cylindrical surface, calculated by multiple aiming ring strategies with sun altitude of 50 degree and sun azimuth of 90 degree. The aim height is at 1,000 cm.

In single aim point strategy, we conclude that the flux distribution be minimum in the direction of the sun. This conclusion contradicts to multiple aim point strategy. Figure 4.27 shows the maximum flux density on the cylindrical surface at various positions when sun azimuth is 90 degree. Consider flux density on cylindrical surface in south (θ_R 0 degree) and north (θ_R 180 degree) direction, the flux density is symmetry. These directions, the flux density is decreased rapidly when sun altitude decrease for 90 degree to 70 degree and almost constant when $\alpha < 75^{\circ}$. In the same direction with the sun (θ_R 90 degree), flux density decreases when sun altitude decrease. When sun altitude is more than 45 degree, flux density in this direction higher than south and north direction.

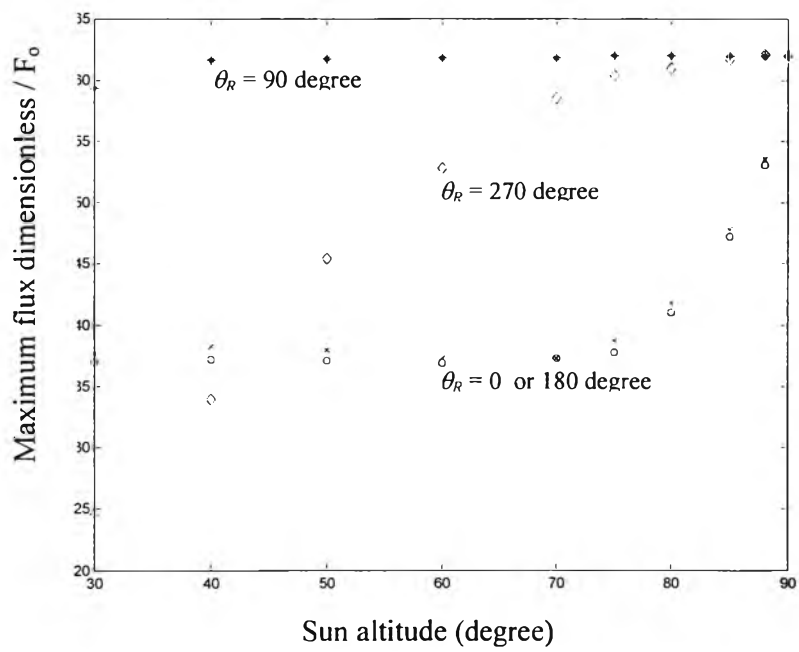

Figure 4.27: Maximum of flux distribution by multiple aim point strategies for sun altitude is 90 degree